DATA SET CATALOG #159

PROGRAM MAGTAL

RA7712

Table of Contents

---

1. INTRODUCTION:

The documentation for this data set was originally on paper, kept in NSSDC's Data Set Catalogs (DSCs). The paper documentation in the Data Set Catalogs have been made into digital images, and then collected into a single PDF file for each Data Set Catalog. The inventory information in these DSCs is current as of July 1, 2004. This inventory information is now no longer maintained in the DSCs, but is now managed in the inventory part of the NSSDC information system. The information existing in the DSCs is now not needed for locating the data files, but we did not remove that inventory information.

The offline tape datasets have now been migrated from the original magnetic tape to Archival Information Packages (AIP's).

A prior restoration may have been done on data sets, if a requestor of this data set has questions; they should send an inquiry to the request office to see if additional information exists.

2. ERRATA/CHANGE LOG:

NOTE: Changes are made in a text box, and will show up that way when displayed on screen with a PDF reader.

When printing, special settings may be required to make the text box appear on the printed output.

Version	Date	Person	Page	Description of Change
01				
02				

3 LINKS TO RELEVANT INFORMATION IN THE ONLINE NSSDC INFORMATION SYSTEM:

http://nssdc.gsfc.nasa.gov/nmc/

[NOTE: This link will take you to the main page of the NSSDC Master Catalog. There you will be able to perform searches to find additional information]

4. CATALOG MATERIALS:

a. Associated Documents To find associated documents you will need to know the document ID number and then click here. http://nssdcftp.gsfc.nasa.gov/miscellaneous/documents/

b. Core Catalog Materials

Nightside Magnetosphere Configuration as Obtained from Trapped Electrons at 1100 Kilometers

DONALD J. WILLIAMS

Johns Hopkins University Applied Physics Laboratory, Silver Spring, Maryland

GILBERT D. MEAD

Goddard Space Flight Center, Greenbelt, Maryland

Abstract. Using data from the polar orbiting satellite 1963 38C, we have obtained the diurnal variation of trapped electrons of energies $E_e \geq 280$ kev and ≥ 1.2 Mev during magnetic quiet. This diurnal variation is measured as a latitude shift for constant electron intensity and is obtained as a function of invariant magnetic latitude. All the data were obtained for dipole orientations within ±12° from the normal to the earth-sun line and for satellite positions within 8° of the noon-midnight meridian. Assuming conservation of the adiabatic invariants as these trapped electrons drift in the magnetosphere, it has been possible to obtain a nightside magnetic field configuration that fits the observed diurnal variations. A dayside configuration that agrees with experimental observations was used. The nightside configuration so determined displays an extended field line geometry and a current sheet in the magnetic equatorial plane. The field due to this current sheet is found to range from 20 to 40 gammas adjacent to the sheet, depending upon the radial extent of the sheet. A field line configuration in the noon-midnight meridian is presented. The nightside trapping boundary as defined by field line closure was found to occur at 1100 km at 67°, in agreement with observed boundaries at 1100 km of ~67° for both ≥40- and ≥280-kev electrons. The situation on the dayside is different and is discussed.

INTRODUCTION

Observations of a diurnal variation in the trapped electron population at high latitudes have been reported by *O'Brien* [1963], *McDiarmid and Burrows* [1964*a* and *b*], and *Frank et al.* [1964]. All these observations were concerned with electrons of energies ≳40 kev, and they showed that the observed diurnal latitudinal shifts at high latitude and low altitude were greater than could be explained by the conservation of the adiabatic invariants in a distorted magnetic field represented by the use of an image dipole [*Malville*, 1960]. *Fairfield* [1964] found that to obtain the large diurnal shifts, it was necessary to add to the dipole field a field normal to the equator but oppositely directed on the dayside and nightside hemispheres, an assumption physically hard to justify.

Measurements of the diurnal shift of ≳280-kev trapped electrons [*Williams and Palmer*, 1965] showed that these higher-energy electrons display a significantly smaller diurnal latitude shift during periods of magnetic quiet than the ≳40-kev electrons do. An initial qualitative analysis by *Williams and Palmer* [1965] suggested that the diurnal shift of ≳280-kev trapped electrons might possibly be explained by invariant conservation in a distorted magnetosphere such as described by *Mead* [1964].

The present, more detailed, quantitative study obtains the latitudinal dependence of the diurnal shift of ≳280-kev and ≳1.2-Mev electrons by determining latitudes of equal flux on the noon and midnight meridians. We find that the addition of a current sheet in the tail of Mead's model, leading to an 'open' field line configuration in the night-side hemisphere, is needed to fit the observed latitude shifts. By an 'open' configuration we simply mean one in which northern and southern high-latitude field lines do not connect, i.e., conjugate-point phenomena are not observed. This nightside field configuration is quite similar to configurations recently suggested by *Dessler and Juday* [1965] and *Axford et al.* [1965], and recently measured by the magnetometer on Imp 1 [*Ness*, 1965].

We thus find that the observed diurnal variations of high-energy ($E_e \geq 280$ kev) trapped

electrons are consistent with the drift of these particles in a distorted magnetosphere under the conservation of the adiabatic invariants μ and J, and the conservation of energy E.

The experimental observations, the magnetospheric distortions, and the experimental and theoretical comparisons are described in subsequent sections.

Experimental Results

Satellite and experiment. A more detailed description of the satellite and the detector may be found in *Williams and Smith* [1965].

Briefly, the data were obtained from the satellite 1963 38C, launched on September 28, 1963, into a nearly circular polar orbit having a 1140-km apogee, 1067-km perigee, 89.9° inclination, and 107.5-minute period. The satellite was magnetically aligned and displayed an oscillation of $<\sim 6°$ about the local line of force some 3 days after launch. Just after launch the satellite orbital plane made an angle of $\sim 6°$ with the noon-midnight meridian and was moving toward the noon-midnight meridian at the approximate rate of 1° per day owing to the earth's motion about the sun.

The detectors of interest comprise an integral electron spectrometer sensitive to electrons in the following energy ranges: $E_e \geq 280$ kev, ≥ 1.2 Mev, ≥ 2.4 Mev, and ≥ 3.6 Mev. The spectrometer detecting channels of interest have full viewing angles of 12° and are oriented to look out normal to the satellite alignment axis. This is well removed from the loss cone at 1100 km, and the spectrometer therefore observes trapped electrons mirroring at the point of observation.

The spectrometer is essentially insensitive to protons of energy $\lesssim 180$ Mev. The monitoring of an onboard proton spectrometer has shown that proton contamination is negligible for the data presented here.

Pertinent information. In trying to arrive at an ambient configuration for the magnetospheric cavity that is consistent with the experimental observations, we have used only data from magnetically quiet periods and have not considered any details of the observed correlation of increases in radiation cavity distortions with increases in magnetospheric distortions as obtained during magnetically active periods [*Williams and Palmer*, 1965].

The data are obtained from October 2 through October 12, 1963, which is the magnetically quiet period used by *Williams and Palmer* [1965] as their period 1. During this time the satellite orbital plane was within 8° of the noon-midnight meridian. Some 47 dayside passes and 28 nightside passes, obtained from the Nasa receiving stations at College, Alaska, and Winkfield, England, have been analyzed. Few, if any, nightside data are available from the remaining stations in our station network.

The data are analyzed in terms of the invariant latitude, Λ, defined at satellite altitude as

$$\cos \Lambda = \sqrt{1.17/L}$$

where L is as defined by *McIlwain* [1961] and is obtained from a 48 coefficient expansion of the earth's magnetic field. Therefore, although still useful as a measure of magnetic latitude in low-altitude orbits, L, as here calculated, loses its significance at altitudes of $\gtrsim 4$ earth radii, where distortions due to the incident solar wind are generally considered to become noticeable. When a more accurate representation of the earth's magnetic field is used in obtaining the parameter L, it becomes apparent that L is no longer constant along a real line of force that reaches out to $\gtrsim 4$ earth radii, and thus offers no conceptual advantage over the second invariant,

$$J = \oint p_\parallel \, ds$$

in these more distant regions.

To avoid confusion, we note here that the values of Λ quoted in *Williams and Palmer* [1965] were obtained from the surface values, $\cos \Lambda = 1/\sqrt{L}$. Those values should be corrected to satellite altitude, as there is a small but noticeable effect ($\sim 1.5°$) in the quoted latitude at which a given latitude shift is observed.

The particles being studied are trapped electrons of energies $E_e \geq 280$ kev and $E_e \geq 1.2$ Mev, having very small equatorial pitch angles. Absolute flux values, accurate to $\sim 20\%$ in the 280-kev and 1.2-Mev channels, may be obtained by multiplying the observed count rates, respectively, by $5(10)^5$ (cm^2 sec ster)$^{-1}$ and 10^5 (cm^2 sec ster)$^{-1}$.

Any dependence of electron intensities on B value is dwarfed by the observed diurnal shift. The B dependence may be expected to be relatively small since, at low altitude and high

B values, a given fractional change in the mirror point B value being observed produces but a very small change in the equatorial pitch angle being sampled [*Williams and Kohl*, 1965].

Data and data analysis. All the data in the interval October 2 through October 12, 1963, were plotted on a scatter plot of count rate versus invariant latitude for both the dayside and nightside hemispheres. Composite curves, representing the average count rates in this time interval, were then constructed from the scatter plots. This process is described and examples are shown in *Williams and Palmer* [1965].

We show in Figure 1 the day and night composite curves for this time interval as obtained by *Williams and Palmer* [1965] but now displayed as a function of latitude. We now include the composite curves for electrons of energy $E_e \geq 1.2$ Mev and see that the higher-energy electrons behave like the 280-kev electrons.

Looking at Figure 1 we see that the separation of the day and night curves can be explained either (*a*) by a vertical shift, i.e., an intensity change in the trapped electron population which is dependent on latitude, or (*b*) by a horizontal (latitude) shift, which is also dependent on latitude, or by both. It turns out that (*a*) requires the establishment of permanent injection mechanisms and/or permanent acceleration mechanisms capable of moving the mirror points of these trapped electrons great distances up and down lines of force. Correspondingly, (*b*) can be accomplished by a shift in latitude of the trapped electron population being observed and might be explained simply by the azimuthal drift of the electrons in a distorted magnetosphere under the conservation of the adiabatic invariants. It is this possible explanation of the observed diurnal shift that we are investigating in this report.

Extending the results of *Madden* [1964], we find that the [illegible] to electric fields associated with magnetic variations yield increases [illegible] at 280 kev. Thus, though important at low energies (~1 kev), these electric fields are apparently unimportant in determining trapped electron behavior at high energies (≳280 kev). Furthermore, Madden shows that such electric fields accelerate electrons so that peak energies are reached at local midnight. This is opposite to the diurnal variation observed by integral threshold detectors where trapped electron intensities are higher at noon than at midnight.

The curves shown in Figure 1 are a good representation of the diurnal shift phenomenon at low altitudes and high latitudes. Although useful results can be obtained from these curves, we believe that more accurate ones can be obtained by using (1) data from 'matched' passes only and (2) data obtained from daily averages of dayside and nightside count rate versus Λ plots. The main reason for our belief is that the curves of Figure 1 are affected by (*a*) slight changes in magnetic activity occurring throughout the time period and (*b*) an uneven distribution of the relative proportion of day and night passes throughout the time interval. The uneven distribution when coupled with the observed steady decay in intensity observed throughout the period under study [*Williams and Smith*, 1965; *Williams and Palmer*, 1965]

Fig. 1. Day and night count rate versus Λ composite curves for the moderately quiet period October 2–12, 1963. Curves are shown for both $E_e \geq 280$ kev and ≥ 1.2 Mev. No night data are available for $\Lambda \lesssim 55°$. Λ is defined at satellite altitude: $\cos \Lambda = \sqrt{1/L}$.

could yield errors in the diurnal shifts as obtained from the composite curves of Figure 1. We find that such errors are indeed small but are noticeable when comparisons are made with predictions of various magnetospheric models. We shall now discuss the data analyses (1) and (2) mentioned above.

1. Matched pass data. It is these data that yield the most accurate results for the values of the diurnal shifts at various latitudes. The matched passes are satellite passes observed by College, Alaska, and Winkfield, England, which, when used in conjunction with each other, trace the satellite from nightside, through the polar region, and on into the dayside hemisphere, or vice versa. Such pairs of passes, being but minutes apart and on reciprocal longitudes, eliminate a great amount of the scatter due to magnetic activity. These matched passes are as close as we are able to come to the ideal of simultaneous observation of the day and nightside latitude profile.

Of the 13 sets of matched passes obtained, College, Alaska, recorded 10 nightside and 3 dayside passes while Winkfield, England, conversely recorded 3 nightside and 10 dayside passes.

Now, assuming that the shifts shown in Figure 1 are due to a shift in latitude of the electron population as it drifts from the dayside to the nightside hemisphere, we have obtained from each of the matched pass pairs, the latitudes where the same count rates were observed on both the noon and midnight meridians. This was done for both the $\geq$280-kev and $\geq$1.2-Mev channels; the results of all the matched passsets are shown in Figure 2 where we have plotted the nighttime latitude Λ_N versus the daytime latitude Λ_D observed for the condition of constant count rate.

Note that, in spite of a certain amount of scatter in the points of Figure 2, there does exist a well-defined latitude dependence of the diurnal variation for high-energy electrons. Also

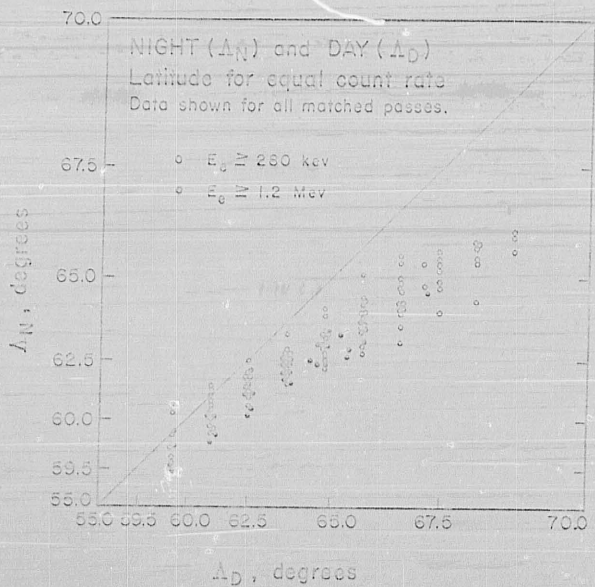

Fig. 2. Plot of Λ_N versus Λ_D for condition of constant count rate. All matched pass data are shown, both for $E_e \geq 280$ kev and $E_e \geq 1.2$ Mev. For the case of no solar wind (a pure dipole field), the data would lie on the $\Lambda_N = \Lambda_D$ line.

TABLE 1. Electron Intensities ($E_e \geq 280$ kev) at $\Lambda = 65.8°$ on Noon-Midnight Meridian throughout October 3, 1963

Noon			Midnight		
Time, UT	Geographic Longitude, °E	Observed Count Rate, c/s	Time, UT	Geographic Longitude, °E	Observed Count Rate, c/s
0020	174	64	0000	358	3
0205	147	55	1048	196	≥1
0542	80	47	1238	169	≥1
1106	12	41	2103	31	1
1255	345	38	2316	8	2
1449	318	87			
1652	291	62			
2336	184	40			

note that the ≥1.2-Mev electrons behave in the same manner as the ≥280-kev electrons. This permits the observation that high-energy electrons in general behave in the same, rather well-defined manner in the outer zone during periods of magnetic quiet.

There is a certain amount of jumpiness in the high-energy electron behavior, to be sure, but in the mean the behavior seems well regulated. It is further illustrated in Table 1, where we show the observed electron intensity at the noon and at the midnight meridian at various times in the day. The representative latitude shown indicates a relatively stable inten-ity at both the noon and midnight meridians throughout the day.

Using the mean values of all the data in Figure 2, we have obtained the amount of latitudinal shift, $\Delta\Lambda = \Lambda_2 - \Lambda_1$ for both $E_e \geq 280$ kev and $E_e \geq 1.2$ Mev, and we show this shift, $\Delta\Lambda$, as a function of daytime latitude in Figure 3. The data in Figure 3 will be compared, in a later section, with the predictions of various magnetic field models. We point out here, once again, the regularity of the mean values of the matched pass points, indicating

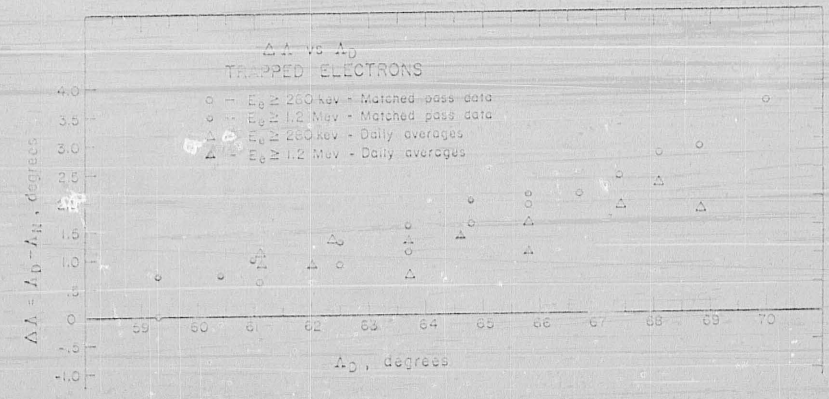

Fig. 3. Plot of the latitude shift, $\Delta\Lambda = \Lambda_2 - \Lambda_1$, versus noontime latitude, Λ_2. Matched pass data points are obtained from the mean values of the data shown in Figure 2. Daily average data points are also mean values obtained from data similar to those shown in Figure 2. See text for discussion. Bars represent entire spread of values observed during the time period October 2–12, 1963.

a well-defined behavior for the electron population during magnetic quiet.

The two representative cases in Figure 3 indicate the entire range of values seen with the data throughout the time period under study.

2. Daily averages. For each 24-hour interval in this time period we constructed the average latitude profile for both $E_e \geq 280$ kev and $E_e \geq 1.2$ Mev for the noon and midnight hemispheres. Using such daily average curves to obtain, on any given day, the daytime and nighttime latitudes, Λ_D and Λ_N, respectively, corresponding to a constant count rate, yields results that are less affected by uneven pass distributions and decay effects than the curves of Figure 1.

This was done for the 11 days of the time interval under study, and the resulting Λ_D and Λ_N values were displayed on a plot similar to that shown in Figure 2 for the matched pass data. The resulting plot was very similar to Figure 2, and we show in Figure 3 the mean values of all the data obtained by the method of daily averages.

We note that the daily average data show somewhat more scatter than the matched pass data, as might be expected since the daily average data will be affected by magnetic variations taking place within a 24-hour period whereas the matched pass data are only affected by magnetic variations taking place within ~30 minutes. Nevertheless, the daily average data do provide an additional check on the accuracy of the matched pass data and are seen to be consistent with the detailed trend of the dependence of the diurnal shift with latitude.

The data in Figure 3 further indicate that electrons of both $E_e \geq 280$ kev and $E_e \geq 1.2$ Mev behave in a similar manner, supporting the previous observation that high-energy electrons in general display the same spatial behavior in the outer zone during periods of magnetic quiet.

Theoretical Considerations

In this section we present calculations of the diurnal shift in latitude of mirroring particles that should be expected, assuming the conservation of the first two invariants and the particle energy. The first or magnetic moment invariant is given by

$$\mu = p_\perp^2/2mB = p^2/2mB_m \qquad (1)$$

in its relativistic form [*Northrop*, 1963]. If energy is conserved, a consequence of the first invariant is that a particle will always mirror at the same value of magnetic field B_m. The only way the mirror point can be raised or lowered for the particle to be scattered or for its energy to change, owing to the presence, for example, of electric fields or time-varying magnetic fields.

The second or longitudinal invariant is given by

$$J = \int_M^{M'} p_\parallel \, ds \qquad (2)$$

where the line integral is taken along the magnetic line of force between the mirror point M and its conjugate M'. Using $p^2 = p_\perp^2 + p_\parallel^2$ and (1), this can be rewritten as

$$J = p \int_M^{M'} \left(1 - \frac{B}{B_m}\right)^{1/2} ds \qquad (3)$$

assuming that p is constant over a bounce period. It is convenient then to define an integral invariant I having the dimensions of a length

$$I = \frac{J}{p} = \int_M^{M'} \left(1 - \frac{B}{B_m}\right)^{1/2} ds \qquad (4)$$

which will be conserved as long as the momentum, and thus the energy, is conserved. This integral is independent of the particle energy and depends only on the mirror point and the magnetic field configuration. If particles do not change energy as they drift around the earth, their mirror points will always be found on a line of constant I. Assuming, of course, that they are not scattered. If loss rates and production rates are slow compared with one drift period (about 1/2 hour for 280-kev electrons at $L = 5$), we would therefore expect to find approximately equal fluxes of mirroring particles at every point of constant B_m and I. The shortest decay times for trapped electrons at these latitudes have been observed to be 1/2 to 1 day, which is more than 10 times as long as the drift times [*Williams and Smith*, 1965].

Under the above set of assumptions, therefore, the problem of predicting the diurnal shift in latitude of mirroring particles reduces to calculating the integral invariant I at constant B_m as a function of latitude, longitude, and local time, and determining the locus of points where I is constant. In the present instance, we may

eliminate the effect of local field irregularities due to nondipolar terms, since the counting rates have been expressed as a function of invariant latitude in an equivalent dipole field. Thus, latitude and local time are the important variables.

To calculate I, we must have a model of the magnetic field. Three such models are used here. The first, given by *Mead* [1964], is based on the solution to the Chapman-Ferraro problem of a solar wind perpendicularly incident on a dipole field. A surface is formed that separates the earth's field from the infinitely conducting, field-free solar wind. The currents on this surface, or magnetopause, modify the field inside the magnetosphere, the major effect being a general compression of the field lines. The resulting distortion of the magnetic field can most conveniently be described in terms of a spherical harmonic expansion, the coefficients determined by making a least-squares fit to the distorted field as calculated at a number of points inside the magnetosphere. The distortion depends on the strength of the solar wind, and in Mead's model the dependence is brought in through the parameter r_0, the distance to the boundary in the solar direction.

The shape of the field lines in the noon-midnight meridian plane is shown in Figure 4 of *Mead* [1964] for the case $r_0 = 10$ earth radii. It is seen there that the effect of field line compression is negligible for lines emerging from latitudes less than 60° ($L = 2$). At higher latitudes the effect becomes significant, and at $\Lambda = 75°$, where the dipole line would normally cross the equator at about 15 earth radii, the equatorial crossing distances in the distorted field are 8.7 and 11.2 earth radii on the noon and midnight meridians, respectively. Thus, the surface currents compress the field lines on both the dayside and the nightside, although not as much on the nightside.

The integral invariants as defined by (4) was calculated as a function of latitude on the noon and midnight meridians for particles mirroring at 1100 km (geocentric distance of 1.17 earth

FIG. 4. Plot of the integral invariant, I, versus field line latitude at 1100 km, Λ, for various magnetospheric configurations. $B_d + B_s$ is the model described by *Mead* [1964]. B_T (60 γ) is an additional constant field component of magnitude 60 γ, solar oriented in the northern hemisphere and antisolar oriented in the southern hemisphere. B_{cb} (40 γ) is a current sheet in the magnetospheric tail yielding a 40-γ field adjacent to the sheet. See text for discussion.

radii). The results for the dipole field plus surface current field (hereafter referred to as B_x to B_z) as given by Mead's model for r_0 = 10 earth radii are shown in Figure 4. The day-night change in latitude for constant B is seen to be about 1° at 70°. Somewhat similar results were obtained by *Midville* [1960], who used an image dipole model for his calculations.

Thus, a simple compression of the magnetosphere by means of surface currents does not predict the observed shifts of several degrees at 70°. However, recent magnetic field measurements by *Ness* [1965] in the tail of the magnetosphere by the Imp 1 satellite has shown that the field configuration in this region is much different from that given by Mead's model. Beyond 10 earth radii, the field in the tail is found to be predominantly in the solar or antisolar direction, instead of perpendicular to the magnetic equator. In addition, a neutral surface separating antisolar directed fields in the southern hemisphere from solar directed fields in the northern hemisphere has been detected over a large area. The presence of such a neutral sheet implies that plasma currents inside the magnetosphere contribute strongly to the magnetic field configuration in the tail region. The presence of such internal plasmas is specifically excluded from the usual Chapman-Ferraro problem, however, suggesting that Mead's model should be modified to take the presence of these plasma currents into consideration.

The simplest way to do this is to vectorially add an additional tail field, B_T, which is directed away from the sun in the southern hemisphere and toward the sun in the northern hemisphere. Such a field would be produced by an infinite sheet of current in the equatorial plane directed opposite to the earth's orbital velocity vector. The integral invariant on the midnight meridian with an additional 60-γ tail field of this type (denoted by $B_x + B_z + B_T$ [60 γ]) has been calculated and is shown in Figure 4.

If the plasma currents producing the additional field in the tail are strongest in the region past 8 or 10 earth radii, the resulting field due to these currents will not be simply directed away from or toward the sun but will also have a southward component opposing the earth's dipole field, as has been pointed out by *Axford et al.* [1965]. Such a configuration can be roughly approximated by a truncated semi-infinite current sheet that does not begin until some distance back of the earth. The geometry is shown in Figure 5. The x axis points away from the sun, and the y axis points south. The field due to such a current sheet is given by

$$B_x = -2J(\theta_2 - \theta_1)$$

$$B_z = 2J \log r_2/r_1$$

where J is the current per unit length in the sheet in electromagnetic units. The current sheet must have both an inner and an outer cutoff to avoid a logarithmic infinity in the value of B_z.

The magnetic field configuration in the noon-midnight meridian plane due to the addition of such a current sheet (the total field denoted by $B_x + B_z + B_T$ [30 γ]) has been calculated. It is shown in Figure 6. The current sheet begins at 10 earth radii back of the earth and cuts off arbitrarily at 40 earth radii. The current strength is such as to produce a field of 30 γ immediately adjacent to the sheet. The major difference between this configuration and Figure 4 of *Mead* [1964] lies in the direction and strength of the field in the tail region. In the earlier model the field lines were roughly perpendicular to the solar direction in the equatorial region. The same is still true in the present model only to about 7 earth radii, but beyond this point the field lines are open and lie parallel to the current sheet. The latitude separating the closed lines from the open lines on

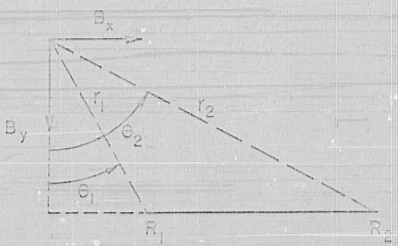

Fig. 5. Diagram showing coordinates used for computation of field due to a truncated semi-infinite current sheet (B_{xz}) coincident with the magnetic equatorial plane and extending radially from R_1 to R_2. It is infinite in length in a direction normal to the paper. The current flow is out of the paper.

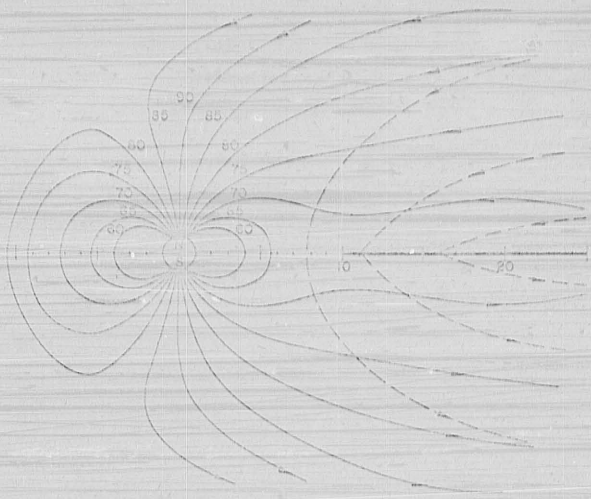

FIG. 6.—Solid lines show the field lines in the noon-midnight meridian plane obtained by adding a current sheet in the tail of the model originally discussed by *Mead* [1964]. This combination was used to obtain the curve labeled $B_0 + B_1 + B_2$, (40 γ) in Figure 4. Dashed lines show field line configuration of the field due to the current sheet alone. Latitudes shown are those at which field lines intersect the surface of the earth. This configuration fits the experimental observations of trapped electron latitude shifts.

the night side is 69° at the earth's surface, or 67° at an altitude of 1100 km in the auroral zone. Therefore we should not expect to find particles trapped above ~67° on the nightside at 1100 km, and the second invariant is no longer defined above this latitude. Note, however, that the position of the 'critical latitude' on the dayside, separating field lines that pass back over the pole into the tail region, is essentially unchanged at about 82° at the earth's surface, well above the auroral zone.

The integral invariant corresponding to this field configuration on the nightside ($B_0 + B_1 + B_{2'}$, [40 γ]) was calculated and is shown in Figure 4. The effect of a finite current sheet producing a 40-γ field is seen to be greater than that of an infinite sheet producing a 40-γ field. The explanation is the presence of the southward component with the finite current sheet. This component, together with the parallel component, is more effective in extending field lines than the parallel component alone. For high-latitude, low-altitude mirroring particles, the integral invariant is essentially a measure of the length of the field line, since the integrand is essentially unity except near the mirror points. Thus, any phenomena that tend to stretch out the field lines on the nightside will enhance the day-night latitude shift. Conversely, anything tending to compress the lines further on the dayside, such as an increase in solar wind intensity, will also enhance the day-night difference. A closer boundary plus a reduced current sheet field would produce about the same results. The configuration on the dayside, however, was chosen to match the observed boundary position of about 10 earth radii in the solar direction during quiet periods.

Discussion

We present in Figure 7 a comparison of the experimental observations of the latitude shift, $\Delta\Lambda$, with the computed shift for various magnetospheric configurations, based on particle drift motions through the magnetosphere under

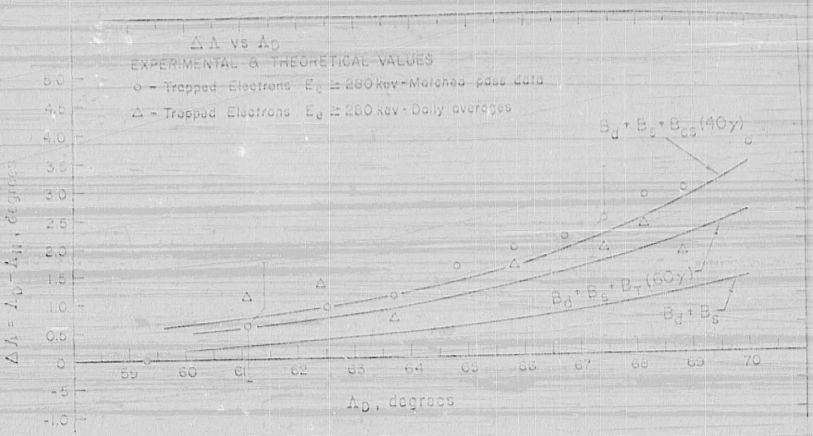

Fig. 7. Comparison of observed latitude shifts with predictions of various magnetic field configurations. All data and calculations are on noon-midnight meridian. The ≥280-kev data points are taken from Figure 3, and they are representative of high-energy electrons in general. The curves are obtained directly from Figure 1 for the field configurations shown.

the conservation of the adiabatic invariants. The theoretical curves shown in this figure are obtained directly from the I versus A curves in Figure 4.

Because both electron energies studied, $E_e \geq 280$ kev and ≥ 1.2 Mev, display the same diurnal variation, we show only the $E_e \geq 280$ kev data in Figure 7 and consider them to be representative of high-energy trapped electrons in general. The bars indicate the entire range of values seen in this time period.

It is clear from Figure 7 that, of the field configurations depicted, the one employing the original model of *Mead* [1964] plus a current sheet located in the magnetospheric tail, $B_d + B_s + B_T$ (40 γ), best fits the experimental observations.

A truncated semi-infinite current sheet will obviously lead to inconsistencies when the field configuration away from the noon-midnight meridian is considered. However, all the data are obtained within 8° of the noon-midnight meridian, and such a current sheet should yield results that might appropriately be compared with the data.

The form of the current sheet, extending radially from 10 to 40 earth radii and being of constant magnitude, is to some degree arbitrary. A more appropriate distribution, one decreasing in magnitude at large radial distances [*Ness*, 1965], might be preferable. In general, moving the front edge of the current sheet closer to the earth's surface, or extending the sheet farther away from the earth and simultaneously lowering the current, will give a satisfactory fit to the data. In Table 2 we show two additional current sheet configurations that also fit the observed trapped-electron diurnal variations.

We note that, although the field strengths near the current sheet agree with some of the measurements reported by *Ness* [1965] in the tail region, they are in general somewhat larger than his observations. For example, Ness shows that the field in the tail region decreases to

TABLE 2. Current Sheet Parameters Yielding Fits to Experimental Observations

Front Edge of Current Sheet, earth radii	Rear Edge of Current Sheet, earth radii	Field Strength Adjacent to Sheet, γ
10	40	40
8	40	35
8	100	23

~10 γ at 30 earth radii, whereas all our values are somewhat larger than this. (The field due to the dipole plus surface currents is negligible in this region.) There are perhaps two reasons for the disagreement. (1) The effects of a ring current have been neglected and will have to be included when more is known about the characteristics of such a source. Outside the ring current the field lines will be extended, but to a greater extent on the nightside hemisphere, thereby reducing the current sheet intensity below the values we found necessary to match the diurnal shifts. (2) A more realistic current distribution should match the observed variation of B with distance from the earth [*Ness*, 1965]. Such a distribution, relatively strong near the earth but weaker in the more distant regions, would probably produce notably the same effect as the current distributions used above.

Nevertheless, the results of this analysis indicate that the nightside geomagnetic field is an 'open' tail configuration and that the current sheet parameters required to fit the trapped electron data are reasonably compatible with the few direct observations available in the nightside magnetic field.

Noon and midnight high-latitude cutoffs for trapped 40-kev electrons have been reported by *O'Brien* [1963], *McDiarmid and Burrows* [1964a], and *Frank et al.* [1964]. All these measurements show the following general characteristics for the high-latitude boundary of trapping for $\geq$40-kev electrons: The average noontime high-latitude cutoff at ~1100 km is in the range $71° \lesssim \Lambda_N \lesssim 76°$, whereas the average midnight boundary at ~1100 km is in the range $67° \lesssim \Lambda_N \lesssim 69°$. Further, using the 40-kev intensity contours given in *Frank et al.* [1964], we have constructed a $\Delta\Lambda$ versus Λ_N plot for $\geq$40-kev electrons in the noon-midnight plane. In Figure 8 we present these results, and, for comparison, the $\geq$280-kev results in Figure 5. Note that Λ_N is given for an altitude of 1100 km. Figure 8 clearly shows that $\geq$40-kev trapped electrons undergo significantly larger diurnal shifts than $\geq$280-kev electrons.

The results of *Williams and Palmer* [1965] indicate that, at an altitude of 1100 km, during times of relative magnetic quiet, the average noontime and midnight high-latitude trapping boundaries for $\geq$280-kev electrons are ~68.5° and ~66°, respectively. Further, the maximum quiet-time noon and midnight trapping boundaries observed were 70° and 67°, respectively. These observations indicate that both $\geq$40- and $\geq$280-kev electrons have a nightside high-latitude trapping boundary of ~67° at 1100 km. This value is in good agreement with the field configuration shown in Figure 6, which yields a nightside latitude boundary of 67° at 1100 km. This latitude corresponds to the low-

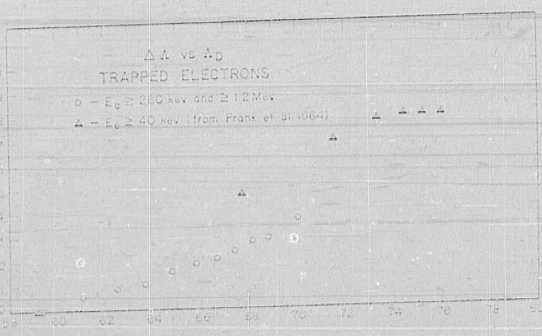

Fig. 8. Comparison of the latitude shifts of $\geq$40- and $\geq$280-kev trapped electrons. The 40-kev data were obtained from the results of *Frank et al.* [1964] and were adjusted to an altitude of 1100 km. The figure shows the significantly larger shifts undergone by the lower-energy trapped electron population.

est latitude field line that displays an 'open' characteristic, i.e., is not connected at the equator.

Thus, the differences in the $\geq$40- and $\geq$280-kev trapped electron spatial characteristics, as shown in Figure 8, seem to be associated with the sunlit hemisphere. It is here that $\geq$40-kev trapped electrons are found at significantly higher latitudes than $\geq$280-kev trapped electrons, in contrast to the nightside situation where the high-latitude boundary is the same for both $\geq$40- and $\geq$280-kev electrons. All this is consistent with the existence of a permanent injection (or acceleration) mechanism on the sunlit part of the magnetosphere. This hypothesis [*O'Brien*, 1963] is further strengthened by observations of a dayside maximum in the $\geq$40-kev precipitated electron intensities [*McDiarmid and Burrows*, 1963*b*; *Frank et al.*, 1964]. The relative behavior of the $\geq$40- and $\geq$280-kev electrons imposes a reasonable energy dependence on the injection processes.

Comparison of the $\geq$40- and $\geq$280-kev electron trapping boundary is subject to uncertainties due to the large temporal variations observed in these intensities. However, the results of *Williams and Palmer* [1965] show that all the $\geq$40-kev data would have to have been obtained from periods of intense magnetic activity to explain the larger shifts observed for the $\geq$40-kev electrons. The $\geq$40-kev observations have, in fact, been taken during periods of low to moderate activity [*O'Brien*, 1963; *McDiarmid and Burrows*, 1963*a* and *b*; *Frank et al.*, 1964], and so the differences do not seem to be due to differences in magnetic activity.

Another source of uncertainty in the relative $\geq$40- and $\geq$280-kev electron trapping boundary is the effect of a varying dipole orientation in the solar wind. The $\geq$280-kev trapped electron data come from within ~8° of the noon-midnight meridian in October, a time when the dipole axis varies ~12° from the normal to the earth-sun line. The $\geq$40-kev data are presumably obtained from all orientations observed and are not knowingly restricted to any preferred orientation. The agreement among the observations at $\geq$40 kev implies that either the dipole orientation produces only a small effect at most or that long enough time intervals were sampled so that reproducible averages over dipole orientation were obtained. In either case, comparisons with the $\geq$280-kev data should be significant.

Summary and Conclusions

The spatial distribution of high-energy ($E \geq 280$ kev) trapped electrons in the outer zone during periods of magnetic quiet is consistent with the drift of these particles through a distorted magnetosphere, under the conservation of the adiabatic invariants. The similarity in the behavior of $\geq$280-kev and $\geq$1.2-Mev trapped electrons allows the above conclusion to extend to high-energy electrons in general.

Detailed observations of the diurnal shift of high-energy trapped electrons ($E \geq 280$ kev and $\geq$1.2 Mev) in the noon-midnight meridian were obtained as a function of invariant latitude during magnetic quiet at a time when the earth's magnetic dipole axis varied ~12° from the normal to the earth-sun line. Then, using a dayside magnetic field configuration chosen to agree with the measurements of *Ness et al.* [1964], a nightside magnetic field configuration was determined by fitting the measurements of the trapped electron diurnal variations. The resulting magnetic field, shown in Figure 6, is seen to have 'open' configuration due to a current sheet located in the magnetic equatorial plane. This current sheet is a truncated semi-infinite sheet extending radially from 10 to 40 earth radii and gives a field strength of 40 γ adjacent to the sheet surface. Field lines due to the sheet alone are also shown in Figure 6. Variations of the current sheet parameters are possible; they are shown in Table 2. This nightside field configuration, as determined by trapped electron behavior at high altitude and low altitude, is quite consistent with the direct magnetic measurements which do exist at $\geq$10 earth radii in the night-side hemisphere [*Ness*, 1965] and agrees closely with the configurations recently suggested by *Dessler and Juday* [1965] and *Axford, Petschek, and Siscoe* [1965].

Therefore, we conclude that the observations of the diurnal variation of high-energy ($E \geq 280$ kev) trapped electrons is consistent with the motion of these electrons in such a distorted magnetosphere under conservation of μ, J, and Φ.

Using this configuration, we can make the further observation that the average behavior of high-energy electrons ($E \geq 280$ kev) dur-

ing magnetic quiet is well cleared and stable, apart from a steady decay of particles from these low-altitude regions. The observed decay rates are in general much longer than the particle drift periods in these regions [*Williams and Palmer*, 1965] and this also imply a certain amount of stability to the trapped population.

Finally, we note that at 1100 km both the ≥40- and the ≥280-kev trapped electrons exhibit a same high-latitude boundary at ~67° at midnight, which agrees well with the high-latitude boundary of closed field lines of 67° in the nightside magnetic field configuration obtained in this study. However, the physical trapping boundary for ≥40-kev electrons extends to significantly higher latitudes than the boundary for ≥280-kev electrons. This yields the larger diurnal shifts obtained for the ≥40-kev electrons [*O'Brien*, 1963; *McDiarmid and Burrows*, 1965*a* and *b*; and *Frank et al.*, 1964] and implies a source mechanism operating on the sunlit hemisphere.

Acknowledgments. We are indebted to Drs. M. P. Nakada, W. N. Hess, and A. J. Dessler. This research was supported in part by the Bureau of Naval Weapons, Department of the Navy, under contract NOw 62-0536-c, and in part by the National Aeronautics and Space Administration Grant.

References

Arnoldy, W. L., H. E. Petschek, and G. L. Stoner, Tail of the geomagnetosphere, *J. Geophys. Res.*, *70*, 1231–1236, 1965.

Dessler, A. J., and R. D. Juday, Configuration of auroral radiation in space, *Planetary Space Sci.*, *13*, 63–72, 1965.

Fairfield, D. H., Trapped particles in a distorted dipole field, *J. Geophys. Res.*, *69*, 3919–3926, 1964.

Frank, L. A., J. A. Van Allen, and J. D. Craven, Large diurnal variations of energetically trapped and of precipitated electrons observed at low altitudes, *J. Geophys. Res.*, *69*, 3155–3167, 1964.

Macris, H., Electric fields in the magnetosphere associated with daily geomagnetic variations and their effects on trapped particles, *Ann. Géophys. Fernet. Phys.*, *20*, 1133–1165, 1964.

McIlwain, C. E., The effect of the initial phase of a magnetic storm upon the outer Van Allen belt, *J. Geophys. Res.*, *69*, 3995–3019, 1964.

McDiarmid, I. B., and J. R. Burrows, High-latitude boundary of the outer radiation zone at 1000 km, *Can. J. Phys.*, *42*, 616–625, 1964*a*.

McDiarmid, I. B., and J. R. Burrows, Diurnal intensity variations in the outer radiation zone at 1000 km, *Can. J. Phys.*, *42*, 1135–1148, 1964*b*.

McIlwain, C. E., Coordinates for mapping the distribution of magnetically trapped particles, *J. Geophys. Res.*, *66*, 3681–3691, 1961.

Mead, G. D., Deformation of the geomagnetic field by the solar wind, *J. Geophys. Res.*, *69*, 1181–1195, 1964.

Ness, N. F., The Earth's magnetic tail, *J. Geophys. Res.*, *70*, 2989–3005, 1965.

Ness, N. F., C. S. Scearce, and J. B. Seek, Initial results of the Imp 1 magnetic field experiment, *J. Geophys. Res.*, *69*, 3531–3569, 1964.

Northrop, T. G., Adiabatic charged particle motion, *Rev. Geophys.*, *1*, 283–304, 1963.

O'Brien, B. J., A large diurnal variation of the geomagnetically trapped radiation, *J. Geophys. Res.*, *68*, 687–695, 1963.

Williams, D. J., and J. W. Kohl, Loss and replenishment of electrons at middle latitudes and high *B* values, *J. Geophys. Res.*, to be published, 1965.

Williams, D. J., and W. F. Palmer, Distortions in the radiation cavity as measured by an 1100-kilometer polar orbiting satellite, *J. Geophys. Res.*, *70*, 557–567, 1965.

Williams, D. J., and A. M. Smith, Daytime trapped electron intensities at high latitudes at 1100 kilometers, *J. Geophys. Res.*, *70*, 541–556, 1965.

(Manuscript received April 14, 1965.)

RA 7712

```
        COMPILER OPTIONS - NAME=  MAIN,OPT=00,LINECNT=58,SOURCE,EBCDIC,NOLIST,NODECK,LOAD,MAP,NOEDIT,ID,XREF
ISN 0002            SUBROUTINE MAGTAL(RR,SINTH,COSTH,SINPHI,COSPHI,RC,R1,R2,BCS,
                   1 BR,BTHETA,BPHI)
                C   FORTRAN IV PROGRAM TO COMPUTE THE EARTHS DIPOLE FIELD DISTORTED BY
                C   THE SOLAR WIND AND GEOMAGNETIC TAIL (JGR 69, 1181, 1964 AND 70,
                C   3017, 1965). SOLAR WIND IS ASSUMED PERPENDICULAR TO DIPOLE AXIS.
                C   INPUT ARE GEOCENTRIC DISTANCE IN EARTH RADII (RR), GEOMAGNETIC
                C   COLATITUDE(SINTH,COSTH), AND LOCAL TIME MEASURED FROM NOON MERIDI-
                C   AN (SINPHI, COSPHI), SUBSOLAR DISTANCE TO MAGNETOPAUSE (RC), DIS-
                C   TANCE TO FRONT AND BACK EDGE OF TAIL CURRENT SHEET (R1 AND R2),
                C   AND MAGNITUDE OF TAIL FIELD ADJACENT TO SHEET (BCS). THUS SUBSOLAR
                C   POINT IS THETA = 90., PHI = 0.  OUTPUT ARE THREE COMPONENTS OF
                C   DISTORTED FIELD, INCLUDING DIPOLE, IN GAMMAS.
ISN 0003            DIMENSION GG(7,7)
ISN 0004            DIMENSION G(7,7),CONST(7,7),P(7,7),DP(7,7),SP(7),CP(7)
ISN 0005            IF(JFIRST - 13) 10,15,10
ISN 0006         10 JFIRST = 13
                C   SET UP INITIAL CONSTANTS THE FIRST TIME AROUND
ISN 0007            DO 5 N=1,7
ISN 0008            DO 5 M=1,7
ISN 0009          5 GG(N,M) = 0.
ISN 0010            NMAX = 7
                C   THE FOLLOWING COEFFICIENTS ARE SCHMIDT-NORMALIZED
ISN 0011            GG(2,1) = -0.25111 E5
ISN 0012            GG(3,2) = -0.12424 E5
ISN 0013            GG(4,1) = -0.00716 E5
ISN 0014            GG(4,3) = -0.02333 E5
ISN 0015            GG(5,2) = -0.02397 E5
ISN 0016            GG(5,4) = -0.00163 E5
ISN 0017            GG(6,1) =  0.00569 E5
ISN 0018            GG(6,3) = -0.01078 E5
ISN 0019            GG(6,5) = -0.00103 E5
ISN 0020            GG(7,2) =  0.00126 E5
ISN 0021            GG(7,4) = -0.00187 E5
ISN 0022            GG(7,6) = -0.00041 E5
ISN 0023            P(1,1) = 1.0
ISN 0024            DP(1,1) = 0.
ISN 0025            SP(1) = 0.
ISN 0026            CP(1) = 1.
ISN 0027            DO 12 N=3,NMAX
ISN 0028            FN = N
ISN 0029            N2 = N - 2
ISN 0030            DO 12 M=1,N2
ISN 0031            FM = M
ISN 0032         12 CONST(N,M) = ((FN-2.)**2 - (FM-1.)**2) / ((2.*FN-3.)*(2.*FN-5.))
ISN 0033            DIMENSION SHMIDT(7,7)
ISN 0034            SHMIDT(1,1) =  1.0
ISN 0035            DO 820 N=2,7
ISN 0036            FN = N
ISN 0037            SHMIDT(N,1) = SHMIDT(N-1,1)*(FN+FN-3.0)/(FN-1.0)
ISN 0038            FACT = 2.0
ISN 0039            DO820 M = 2,N
ISN 0040            FM = M
ISN 0041            SHMIDT(N,M) = SHMIDT(N,M-1)*SQRT ((FN-FM+1.0)*FACT/(FN+FM-2.0))
ISN 0042         820 FACT = 1.0
ISN 0043          15 IF(RC-ROOLD) 16,20,16
ISN 0044          16 ROOLD = RC
```

```
ISN 0045          DIMENSION FAC(7)
ISN 0046          FAC(2) = RO**3
ISN 0047          DO 17 N=3,NMAX
ISN 0048       17 FAC(N) = RO * FAC(N-1)
ISN 0049          DO 18 N=2,NMAX
ISN 0050          DO 18 M=1,N
ISN 0051       18 G(N,M) = SHMIDT(N,M) * GG(N,M) / FAC(N)
ISN 0052       20 CONTINUE
                C     BEGIN CALCULATION FOR SPECIFIED INPUT
ISN 0053       30 CT = COSTH
ISN 0054          ST = SINTH
ISN 0055          SP(2) = SINPHI
ISN 0056          CP(2) = COSPHI
                C     CALCULATE SIN(M*PHI) AND COS(M*PHI)
ISN 0057          DO 41 M=3,NMAX
ISN 0058          SP(M) = SP(2)*CP(M-1) + CP(2)*SP(M-1)
ISN 0059       41 CP(M) = CP(2)*CP(M-1) - SP(2)*SP(M-1)
ISN 0060          R = RR
ISN 0061          A = 1.
ISN 0062          RA = R/A
ISN 0063          ROA = 1.
ISN 0064          BR = 0.
ISN 0065          BTHETA = 0.
ISN 0066          BPHI = 0.
ISN 0067          FN = 1.
                C     CALCULATE SPHERICAL HARMONICS FOR CAVITY FIELD
ISN 0068          DO 50 N=2,NMAX
ISN 0069          SUMR = 0.
ISN 0070          SUMT = 0.
ISN 0071          SUMP = 0.
ISN 0072          FM = 0.
                C     DEVELOP LEGENDRE FUNCTIONS AND THEIR DERIVATIVES BY RECURSION FORMULAE
ISN 0073          DO 49 M=1,N
ISN 0074          IF(N-M-1) 44,43,42
ISN 0075       42 P(N,M) = CT*P(N-1,M) - CONST(N,M)*P(N-2,M)
ISN 0076          DP(N,M) = CT*DP(N-1,M) - ST*P(N-1,M) - CONST(N,M)*DP(N-2,M)
ISN 0077          GO TO 45
ISN 0078       43 P(N,M) = CT * P(N-1,M)
ISN 0079          DP(N,M) = CT*DP(N-1,M) - ST*P(N-1,M)
ISN 0080          GO TO 45
ISN 0081       44 P(N,N) = ST * P(N-1,N-1)
ISN 0082          DP(N,N) = ST*DP(N-1,N-1) + CT*P(N-1,N-1)
ISN 0083       45 CONTINUE
ISN 0084          TS = G(N,M) * CP(M)
ISN 0085          SUMR = SUMR + P(N,M)*TS
ISN 0086          SUMT = SUMT + DP(N,M)*TS
ISN 0087          SUMP = SUMP + FM*P(N,M)*G(N,M)*SP(M)
ISN 0088          FM = FM + 1.
ISN 0089       49 CONTINUE
ISN 0090          BR = BR - ROA*FN*SUMR
ISN 0091          BTHETA = BTHETA - ROA*SUMT
ISN 0092          BPHI = BPHI + ROA*SUMP
ISN 0093          ROA = ROA * RA
ISN 0094          FN = FN + 1.
ISN 0095       50 CONTINUE
ISN 0096          BPHI = BPHI / ST
```

```
C       ADD DIPOLE FIELD TO CAVITY FIELD
ISN 0097        R3 = R**3
ISN 0098        BR = BR -62000. * COSTH / R3
ISN 0099        BTHETA = BTHETA - 31000. * SINTH / R3
C       CALCULATE TAIL FIELD
ISN 0100        IF(BCS.EQ.0.) RETURN
ISN 0102        RCT = R * CT
ISN 0103        RCT2 = RCT**2
ISN 0104        RSC = R * ST * CP(2)
ISN 0105        TOP = R2 + RSC
ISN 0106        BOT = R1 + RSC
ISN 0107        BX = -BCS * (ATAN(TOP/RCT) - ATAN(BOT/RCT)) / 3.14159265
ISN 0108        BPHI = BPHI + BX * SP(2)
ISN 0109        BRHO = -BX * CP(2)
ISN 0110        BY = BCS * ALOG((RCT2+TOP**2)/(RCT2+BOT**2)) / 6.28318531
ISN 0111        BR = BR + BRHO*ST - BY*CT
ISN 0112        BTHETA = BTHETA + BRHO*CT + BY*ST
ISN 0113    60  RETURN
ISN 0114        END
```

*****F O R T R A N C R O S S R E F E R E N C E L I S T I N G*****

SYMBOL	INTERNAL STATEMENT NUMBERS
A	0061 0062
G	0004 0051 0084 0087
M	0008 0009 0030 0031 0032 0039 0040 0041 0041 0050 0051 0051 0051 0057 0058 0058 0058 0059 0059
	0059 0073 0074 0075 0075 0075 0075 0076 0076 0076 0076 0078 0078 0079 0079 0079 0084 0084
	0085 0086 0087 0087 0087
N	0007 0009 0027 0028 0029 0032 0035 0036 0037 0037 0039 0041 0041 0047 0048 0048 0049 0050 0051
	0051 0051 0051 0068 0073 0074 0075 0075 0075 0075 0076 0076 0076 0076 0076 0078 0078 0079 0079
	0079 0081 0081 0081 0081 0082 0082 0082 0082 0082 0082 0084 0085 0086 0087 0087
P	0004 0023 0075 0075 0075 0076 0078 0078 0079 0081 0081 0082 0085 0087
R	0060 0062 0097 0102 0104
BR	0002 0064 0090 0090 0098 0098 0111 0111
BX	0107 0108 0109
BY	0110 0111 0112
CP	0004 0026 0056 0058 0058 0059 0059 0059 0084 0104 0109
CT	0053 0075 0076 0078 0079 0082 0102 0111 0112
DP	0004 0026 0076 0076 0076 0079 0079 0082 0082 0086
FM	0031 0032 0040 0041 0041 0072 0087 0088 0088
FN	0028 0032 0032 0032 0036 0037 0037 0037 0041 0041 0067 0090 0094 0094
GG	0003 0009 0011 0012 0013 0014 0015 0016 0017 0018 0019 0020 0021 0022 0051
N2	0029 0030
RA	0062 0093
RO	0002 0043 0044 0046 0048
RR	0002 0060
R1	0002 0106
R2	0002 0105
R3	0097 0098 0099
SB	0004 0028 0055 0059 0058 0058 0059 0059 0087 0108
ST	0054 0074 0079 0081 0092 0096 0104 0111 0112
TS	0084 0085 0085
BCS	0002 0100 0107 0110
BCT	0105 0107 0110
FAC	0045 0046 0048 0048 0051
RCT	0102 0103 0107 0107
ROA	0063 0090 0091 0092 0093 0093
RSC	0104 0105 0106
TOP	0105 0107 0110
ALOG	0110
ATAN	0107 0107
BPHI	0002 0066 0092 0092 0096 0096 0108 0108
BRHO	0109 0111 0112
FACT	0038 0041 0042
NMAX	0010 0027 0047 0049 0057 0068
RCT2	0103 0110 0110
SQRT	0041
SUMP	0071 0087 0087 0092
SUMR	0069 0085 0085 0090
SUMT	0070 0086 0086 0091
CONST	0004 0032 0075 0076
COSTH	0002 0053 0098
ROOLD	0043 0044
SINTH	0002 0054 0099
RTHETA	0002 0065 0091 0091 0099 0099 0112 0112
COSPHI	0002 0056
JFIRST	0005 0006

SYMBOL	INTERNAL STATEMENT NUMBERS						
MAGTAL	0002						
SHMIDT	0033	0034	0037	0037	0041	0041	0051
SINPHI	0002	0055					

LABEL	DEFINED	REFERENCES	
5	0009	0007	0008
10	0006	0005	0005
12	0032	0027	0030
15	0043	0005	
16	0044	0043	0043
17	0048	0047	
18	0051	0045	0050
20	0052	0043	
30	0053		
41	0059	0057	
42	0075	0074	
43	0078	0074	
44	0081	0074	
45	0083	0077	0080
49	0089	0073	
50	0095	0068	
50	0113		
820	0042	0035	0039

NAME	TAG	TYPE	ADD.
A	SF	R*4	000118
P	SF	R*4	000280
BY	SF	R*4	000130
FM	SFA	R*4	000138
R1	SF	R*4	000144
R2	F	R*4	000154
TS	SF	R*4	000160
RCT	SFA	R*4	00016C
BPHI	SF	R*4	00017C
RCT2	SFA	R*4	000180
CONST	SF	R*4	000520
ALOG	XF	R*4	000000
COSPHI	F	R*4	0001AC
SINPHI	F	R*4	000188

NAME	TAG	TYPE	ADD.
G	SF	R*4	0001BC
R	SF	R*4	000124
CP	SF	R*4	000344
FN	SFA	R*4	00013C
R0	F	R*4	000148
R3	SF	R*4	000158
BCS	F	R*4	000164
R0A	SF	R*4	000170
BRHO	SF	R*4	000180
SUMP	SF	R*4	000190
COSTH	F	R*4	00019C
ATAN	XF	R*4	000000
JFIRST	S	I*4	0001B0

NAME	TAG	TYPE	ADD.
M	SF	I*4	00011C
BR	SF	R*4	000128
CT	SF	R*4	000134
GG	SF	R*4	000424
RR	F	R*4	00014C
SP	SF	R*4	0004E8
BOT	SFA	R*4	000168
BSC	SF	R*4	000174
FACT	SFA	R*4	000184
SUMR	SF	R*4	000194
ROOLD	S	R*4	0001A0
SORT	XF	R*4	000000
MAGTAL		I*4	0001B4

NAME	TAG	TYPE	ADD.
N	SF	I*4	000120
BX	SF	R*4	00012C
DP	SF	R*4	000360
N2	SF	I*4	000140
R1	F	R*4	000150
ST	SF	R*4	00015C
FAC	SF	R*4	000504
TOP	SFA	R*4	000178
NMAX	SF	I*4	000188
SUMT	SF	R*4	000198
SINTH	F	R*4	0001A4
BTHETA	SF	R*4	0001A8
SHMIDT	SF	R*4	0005E4

LABEL	ADDR	LABEL	ADDR	LABEL	ADDR	LABEL	ADDR
10	00076A	5	000782	12	0008E4	820	000AEE
15	000822	16	000836	17	000850	18	000B9A
20	000C42	30	000C42 NR	41	000CB6	42	000D92
43	000EEC	44	000FAA	45	001060	49	00115A
50	0011C0	60	001384 NR				

OPTIONS IN EFFECT NAME= MAIN,OPT=00,LINECNT=58

OPTIONS IN EFFECT SOURCE,EBCDIC,NOLIST,NODECK,LOAD,MAP,NOEDIT,ID,XREF

STATISTICS SOURCE STATEMENTS = 113 ,PROGRAM SIZE = 5176

STATISTICS NO DIAGNOSTICS GENERATED

****** END OF COMPILATION ******

```
IEF285I   SYS71230.T160946.RV000.YZ2RMCD1.OBJMOD        PASSED
IEF285I   VOL SER NOS= K3SCR2.
IEF285I   SYS71230.T160946.SV000.YZ2RMCD1.R0000391      SYSOUT
IEF285I   VOL SER NOS= K3SCR5.
IEF285I   SYS71230.T160946.SV000.YZ2RMCD1.R0000392      DELETED
IEF285I   VOL SER NOS= K3SCR4.
IEF285I   SYS71230.T160946.RV000.YZ2RMCD1.R0000393      DELETED
IEF285I   VOL SER NOS= K3SCR2.
IEF285I   SYS71230.T160946.RV000.YZ2RMCD1.R0000394      DELETED
IEF285I   VOL SER NOS= K3SCR2.
IEF285I   SYS71230.T160946.SV000.YZ2RMCD1.R0000395      DELETED
IEF285I   VOL SER NOS= K3SCR5.
IEF285I   SYS71230.T160946.RV000.YZ2RMCD1.S0000396      SYSIN
IEF285I   VOL SER NOS= K3SCR3.
IEF285I   SYS71230.T160946.RV000.YZ2RMCD1.S0000396      DELETED
IEF285I   VOL SER NOS= K3SCR3.
IEF373I STEP /SOURCE  / START 71230.1737
IEF374I STEP /SOURCE  / STOP  71230.1753 CPU  00MIN 02.45SEC MAIN 248K LCS   0K
                                                    STEP TIME =     .11 MINS=(CPU=     .04,IO=     .07)
- STEP 01 -     RETURN CODE = 0000
                                  IO IN SECS. DISK=    4.26.DRUM=     .11,TAPE=     .00.CELL=     .00.OTHR=     .28

IEF285I   SYS71230.T160946.RV000.YZ2RMCD1.OBJMOD        DELETED
IEF285I   VOL SER NOS= K3SCR2.
IEF375I  JOB /YZ2RMCD1/ START 71230.1737
IEF376I  JOB /YZ2RMCD1/ STOP  71230.1753 CPU  00MIN 02.45SEC
                                                                    TIME=17.53.52.55 DATE=08-18-71
-  SYSTEM=MVT-18 (12-07-69)   K3
                                                    TOTAL TIME =    .11 MINS=(CPU=     .04,IO=     .07)
- JOB 0323-
                                  IO IN SECS. DISK=    4.26.DRUM=     .11,TAPE=     .00.CELL=     .00.OTHR=     .28
```

```
//YZJRJRWP JOB (K100523,SL,P,KA0003,002002),039,MSGLEVEL=1                  03980005
//STEP1 EXEC FORTRANH
XXDEFAULT PROC FORTRAN=IEKAA00,NBLK=40          * FORTRANH * 19 NOV 71 *  00000010
XXSOURCE EXEC PGM=&FORTRAN,REGION=320K,PARM='OPT=1'                       00000020
IEF653I SUBSTITUTION JCL - PGM=IEKAA00,REGION=320K,PARM='OPT=1'
XXSTEPLIB DD DSN=SYS1.FORTH,DISP=SHR                                      00000030
XXSYSLIN DD DSN=&&OBJMOD,DISP=(MOD,PASS),UNIT=2314,                       00000040
XX SPACE=(3200,(&NBLK,40),,,ROUND),DCB=(RECFM=FB,LRECL=80,BLKSIZE=3200)   00000050
IEF653I SUBSTITUTION JCL - SPACE=(3200,(40,40),,,ROUND),DCB=(RECFM=FB,LRECL=80,BLKSIZE=3200)
XXSYSPRINT DD SYSOUT=A,UNIT=(2314,SEP=SYSLIN),                            00000060
XX DCB=(RECFM=VBA,LRECL=137,BLKSIZE=7265)                                 00000070
XXSYSPUNCH DD SYSOUT=B,DCB=(RECFM=FB,LRECL=80,BLKSIZE=3200)               00000080
XXSYSUT1 DD UNIT=(2314,SEP=(SYSLIN,SYSPRINT)),SPACE=(CYL,(1,1))           00000090
XXSYSUT2 DD UNIT=(2314,SEP=(SYSLIN,SYSPRINT,SYSUT1)),SPACE=(CYL,(1,1))    00000100
//SOURCE.SYSIN DD *
//
IEF236I ALLOC. FOR YZJRJRWP SOURCE    STEP1
IEF237I 1C0    ALLOCATED TO STEPLIB
IEF237I 213    ALLOCATED TO SYSLIN
IEF237I 217    ALLOCATED TO SYSPRINT
IEF237I 213    ALLOCATED TO SYSPUNCH
IEF237I 232    ALLOCATED TO SYSUT1
IEF237I 216    ALLOCATED TO SYSUT2
IEF237I 213    ALLOCATED TO SYSIN
```

```
      COMPILER OPTIONS - NAME= MAIN,OPT=01,LINECNT=58,SOURCE,EBCDIC,NOLIST,NODECK,LOAD,MAP,NOEDIT,ID,NOXREF
ISN 0002              SUBROUTINE MAGTAL(RR,SINTH,COSTH,SINPHI,COSPHI,RO,R1,R2,BCS,
                     1 BR,BTHETA,BPHI)
                    C     FORTRAN IV PROGRAM TO COMPUTE THE EARTHS DIPOLE FIELD DISTORTED BY
                    C     THE SOLAR WIND AND GEOMAGNETIC TAIL (JGR 69, 1181, 1964 AND 70,
                    C     3017, 1965). SOLAR WIND IS ASSUMED PERPENDICULAR TO DIPOLE AXIS.
                    C     INPUT ARE GEOCENTRIC DISTANCE IN EARTH RADII (RR), GEOMAGNETIC
                    C     COLATITUDE(SINTH,COSTH), AND LOCAL TIME MEASURED FROM NOON MERIDI-
                    C     AN (SINPHI, COSPHI), SUBSOLAR DISTANCE TO MAGNETOPAUSE (RO), DIS-
                    C     TANCE TO FRONT AND BACK EDGE OF TAIL CURRENT SHEET (R1 AND R2),
                    C     AND MAGNITUDE OF TAIL FIELD ADJACENT TO SHEET (BCS). THUS SUBSOLAR
                    C     POINT IS THETA = 90., PHI = 0.  OUTPUT ARE THREE COMPONENTS OF
                    C     DISTORTED FIELD, INCLUDING DIPOLE, IN GAMMAS.
ISN 0003              DIMENSION GG(7,7)
ISN 0004              DIMENSION G(7,7),CONST(7,7),P(7,7),DP(7,7),SP(7),CP(7)
ISN 0005              IF(JFIRST - 13) 10,15,10
ISN 0006           10 JFIRST = 13
                    C     SET UP INITIAL CONSTANTS THE FIRST TIME AROUND
ISN 0007              DO 5 N=1,7
ISN 0008              DO 5 M=1,7
ISN 0009            5 GG(N,M) = 0.
ISN 0010              NMAX = 7
                    C     THE FOLLOWING COEFFICIENTS ARE SCHMIDT-NORMALIZED
ISN 0011              GG(2,1) = -0.25111 E5
ISN 0012              GG(3,2) = -0.12424 E5
ISN 0013              GG(4,1) = -0.00716 E5
ISN 0014              GG(4,3) = -0.02333 E5
ISN 0015              GG(5,2) = -0.02397 E5
ISN 0016              GG(5,4) = -0.00163 E5
ISN 0017              GG(6,1) =  0.00569 E5
ISN 0018              GG(6,3) = -0.01078 E5
ISN 0019              GG(6,5) = -0.00103 E5
ISN 0020              GG(7,2) =  0.00126 E5
ISN 0021              GG(7,4) = -0.00187 E5
ISN 0022              GG(7,6) = -0.00041 E5
ISN 0023              P(1,1) = 1.0
ISN 0024              DP(1,1) = 0.
ISN 0025              SP(1) = 0.
ISN 0026              CP(1) = 1.
ISN 0027              DO 12 N=3,NMAX
ISN 0028              FN = N
ISN 0029              N2 = N - 2
ISN 0030              DO 12 M=1,N2
ISN 0031              FM = M
ISN 0032           12 CONST(N,M) = ((FN-2.)**2 - (FM-1.)**2) / ((2.*FN-3.)*(2.*FN-5.))
ISN 0033              DIMENSION SHMIDT(7,7)
ISN 0034              SHMIDT(1,1) = 1.0
ISN 0035              DO 820 N=2,7
ISN 0036              FN = N
ISN 0037              SHMIDT(N,1) = SHMIDT(N-1,1)*(FN+FN-3.0)/(FN-1.0)
ISN 0038              FACT = 2.0
ISN 0039              DO820 M = 2,N
ISN 0040              FM = M
ISN 0041              SHMIDT(N,M) = SHMIDT(N,M-1)*SQRT ((FN-FM+1.0)*FACT/(FN+FM-2.0))
ISN 0042           820 FACT = 1.0
ISN 0043           15 IF(RO-ROOLD) 16,20,16
ISN 0044           16 ROOLD = RO
```

```
ISN 0045          DIMENSION FAC(7)
ISN 0046          FAC(2) = RO**3
ISN 0047          DO 17 N=3,NMAX
ISN 0048       17 FAC(N) = RO * FAC(N-1)
ISN 0049          DO 18 N=2,NMAX
ISN 0050          DO 18 M=1,N
ISN 0051       18 G(N,M) = SHMIDT(N,M) * GG(N,M) / FAC(N)
ISN 0052       20 CONTINUE
               C     BEGIN CALCULATION FOR SPECIFIED INPUT
ISN 0053       30 CT = COSTH
ISN 0054          ST = SINTH
ISN 0055          SP(2) = SINPHI
ISN 0056          CP(2) = COSPHI
               C     CALCULATE SIN(M*PHI) AND COS(M*PHI)
ISN 0057          DO 41 M=3,NMAX
ISN 0058          SP(M) = SP(2)*CP(M-1) + CP(2)*SP(M-1)
ISN 0059       41 CP(M) = CP(2)*CP(M-1) - SP(2)*SP(M-1)
ISN 0060          R = RR
ISN 0061          A = 1.
ISN 0062          RA = R/A
ISN 0063          RDA = 1.
ISN 0064          DR = 0.
ISN 0065          BTHETA = 0.
ISN 0066          BPHI = 0.
ISN 0067          FN = 1.
               C     CALCULATE SPHERICAL HARMONICS FOR CAVITY FIELD
ISN 0068          DO 50 N=2,NMAX
ISN 0069          SUMR = 0.
ISN 0070          SUMT = 0.
ISN 0071          SUMP = 0.
ISN 0072          FM = 0.
               C     DEVELOP LEGENDRE FUNCTIONS AND THEIR DERIVATIVES BY RECURSION FORMULAE
ISN 0073          DO 49 M=1,N
ISN 0074          IF(N-M-1) 44,43,42
ISN 0075       42 P(N,M) = CT*P(N-1,M) - CONST(N,M)*P(N-2,M)
ISN 0076          DP(N,M) = CT*DP(N-1,M) - ST*P(N-1,M) - CONST(N,M)*DP(N-2,M)
ISN 0077          GO TO 45
ISN 0078       43 P(N,M) = CT * P(N-1,M)
ISN 0079          DP(N,M) = CT*DP(N-1,M) - ST*P(N-1,M)
ISN 0080          GO TO 45
ISN 0081       44 P(N,N) = ST * P(N-1,N-1)
ISN 0082          DP(N,N) = ST*DP(N-1,N-1) + CT*P(N-1,N-1)
ISN 0083       45 CONTINUE
ISN 0084          TS = G(N,M) * CP(M)
ISN 0085          SUMR = SUMR + P(N,M)*TS
ISN 0086          SUMT = SUMT + DP(N,M)*TS
ISN 0087          SUMP = SUMP + FM*P(N,M)*G(N,M)*SP(M)
ISN 0088          FM = FM + 1.
ISN 0089       49 CONTINUE
ISN 0090          BR = BR - RDA*FN*SUMR
ISN 0091          BTHETA = BTHETA - RDA*SUMT
ISN 0092          BPHI = BPHI + RDA*SUMP
ISN 0093          RDA = RDA * RA
ISN 0094          FN = FN + 1.
ISN 0095       50 CONTINUE
ISN 0096          BPHI = BPHI / ST
```

```
      C     ADD DIPOLE FIELD TO CAVITY FIELD
ISN 0097    R3 = R**3
ISN 0098    BR = BR -62000. * COSTH / R3
ISN 0099    BTHETA = BTHETA - 31000. * SINTH / R3
      C     CALCULATE TAIL FIELD
ISN 0100    IF(BCS.EQ.0.) RETURN
ISN 0102    RCT = R * CT
ISN 0103    RCT2 = RCT**2
ISN 0104    RSC = R * ST * CP(2)
ISN 0105    TOP = R2 + RSC
ISN 0106    BOT = R1 + RSC
ISN 0107    BX = -BCS * (ATAN(TOP/RCT) - ATAN(BOT/RCT)) / 3.14159265
ISN 0108    BPHI = BPHI + BX * SP(2)
ISN 0109    BRHO = -BX * CP(2)
ISN 0110    BY = BCS * ALOG((RCT2+TOP**2)/(RCT2+BOT**2)) / 6.28318531
ISN 0111    BR = BR + BRHO*ST - BY*CT
ISN 0112    BTHETA = BTHETA + BRHO*CT + BY*ST
ISN 0113   60 RETURN
ISN 0114    END
```

NAME	TAG	TYPE	ADD.	NAME	TAG	TYPE	ADD.	NAME	TAG	TYPE	ADD.	NAME	TAG	TYPE	ADD.
A	SF	R*4	000118	G	SF	R*4	0001BC	M	SF	I*4	00011C	N	SF	I*4	000120
B	SF	R*4	000280	R	SF	R*4	000124	BR	SF	R*4	000128	BX	SF	R*4	00012C
BY	SF	R*4	000130	CP	SF	R*4	000344	CT	SF	R*4	000134	DP	SF	R*4	000360
FM	SFA	R*4	000138	FN	SFA	R*4	00013C	GG	SF	R*4	000424	N2	SF	I*4	000140
RA	SF	R*4	000144	RO	F	R*4	000148	RR	F	R*4	00014C	R1	F	R*4	000150
R2	F	R*4	000154	R3	SF	R*4	000158	SP	SF	R*4	0004E8	ST	SF	R*4	00015C
TS	SF	R*4	000160	BCS	F	R*4	000164	BOT	SFA	R*4	000168	FAC	SF	R*4	000504
RCT	SFA	R*4	00016C	ROA	SF	R*4	000170	RSC	SF	R*4	000174	TOP	SFA	R*4	000178
BPHI	SF	R*4	00017C	BRHO	SF	R*4	000180	FACT	SFA	R*4	000184	NMAX	SF	I*4	000188
RCT2	SFA	R*4	000184	SUMP	SF	R*4	000190	SUMR	SF	R*4	000194	SUMT	SF	R*4	000198
CONST	SF	R*4	000520	COSTH	F	R*4	00019C	RODLO	S	R*4	0001A0	SINTH	F	R*4	0001A4
ALOG	XF	R*4	000000	ATAN	XF	R*4	000000	SQRT	XF	R*4	000000	BTHETA	SF	R*4	0001A8
COSPHI	F	R*4	0001AC	JFIRST	S	I*4	0001B0	MAGTAL		I*4	0001B4	SHMIDT	SF	R*4	0005E4
SINPHI	F	R*4	0001B8												

LABEL	ADDR	LABEL	ADDR	LABEL	ADDR	LABEL	ADDR
10	0006F0	5	0005F0	12	00082A	820	000984
15	0009AE	16	0009BE	17	0009DC	18	000A12
20	000A7E	30	000A7E NR	41	000AD4	42	000B78
43	000C42	44	000CB8	45	000D2A	49	000DD4
50	000E36	60	000FB2 NR				

OPTIONS IN EFFECT NAME= MAIN,OPT=01,LINECNT=58

OPTIONS IN EFFECT SOURCE,EBCDIC,NOLIST,NODECK,LOAD,MAP,NOEDIT,ID,NOXREF

STATISTICS SOURCE STATEMENTS = 113 ,PROGRAM SIZE = 4194

STATISTICS NO DIAGNOSTICS GENERATED

****** END OF COMPILATION ******

```
IEF285I   SYS1.FORTH                                      KEPT
IEF285I   VOL SER NOS= M2DRM1.
IEF285I   SYS71361.T191747.RV000.YZJRJRWP.OBJMOD          PASSED
IEF285I   VOL SER NOS= M2SCR5.
IEF285I   SYS71361.T191747.SV000.YZJRJRWP.R0000055        SYSOUT
IEF285I   VOL SER NOS= M2SCR1.
IEF285I   SYS71361.T191747.SV000.YZJRJRWP.R0000056        DELETED
IEF285I   VOL SER NOS= M2SCR5.
IEF285I   SYS71361.T191747.RV000.YZJRJRWP.R0000057        DELETED
IEF285I   VOL SER NOS= M2SCR6.
IEF285I   SYS71361.T191747.RV000.YZJRJRWP.R0000058        DELETED
IEF285I   VOL SER NOS= M2SCR4.
IEF285I   SYS71361.T191747.RV000.YZJRJRWP.S0000059        SYSIN
IEF285I   VOL SER NOS= M2SCR5.
IEF285I   SYS71361.T191747.RV000.YZJRJRWP.S0000059        DELETED
IEF285I   VOL SER NOS= M2SCR5.
IEF373I STEP /SOURCE  / START 71361.2015
IEF374I STEP /SOURCE  / STOP  71361.2016 CPU  00MIN 01.10SEC MAIN 296K LCS   0K
- STEP 01 -     RETURN CODE = 0000                    STEP TIME =     .04 MINS=(CPU=     .01,IO=     .03)
                                          IO IN SECS. DISK=    2.24,DRUM=     .14,TAPE=     .00,CELL=     .00,OTHR=     .32
IEF285I   SYS71361.T191747.RV000.YZJRJRWP.OBJMOD          DELETED
IEF285I   VOL SER NOS= M2SCR5.
IEF375I  JOB /YZJRJRWP/ START 71361.2015
IEF376I  JOB /YZJRJRWP/ STOP  71361.2016 CPU  00MIN 01.10SEC
-  SYSTEM=MVT-18 (12-07-69)   M2                                        TIME=20.16.14.74 DATE=12-27-71
- JOB 0627-                                    TOTAL TIME =     .04 MINS=(CPU=     .01,IO=     .03)
                                          IO IN SECS. DISK=    2.24,DRUM=     .14,TAPE=     .00,CELL=     .00,OTHR=     .32
```